PAPER

Simulation of RF Noise in MOSFETs Using Different Transport Models

Andreas SCHENK[†a)], **Bernhard SCHMITHÜSEN**[†], **Andreas WETTSTEIN**[††], **Axel ERLEBACH**[††], **Simon BRUGGER**[†], **Fabian M. BUFLER**[†], **Thomas FEUDEL**[†††], ***and*** **Wolfgang FICHTNER**[†], ***Nonmembers***

SUMMARY RF noise in quarter-micron nMOSFETs is analysed on the device level based on Shockley's impedance field method. The impact of different transport models and physical parameters is discussed in detail. Well-calibrated drift-diffusion and energy-balance models give very similar results for noise current spectral densities and noise figures. We show by numerical simulations with the general-purpose device simulator DESSIS$_{-\mathrm{ISE}}$ that the hot-electron effect on RF noise is unimportant under normal operating conditions and that thermal substrate noise is dominant below 0.5 GHz. The contribution of energy-current fluctuations to the terminal noise is found to be negligible. Application of noise sources generated in bulk full-band Monte Carlo simulations changes the noise figures considerably, which underlines the importance of proper noise source models for far-from-equilibrium conditions.

key words: *device simulation, RF noise, impedance field method, Langevin equation*

1. Introduction

The reliability and functionality of modern semiconductor devices is, to a certain extent, determined by the statistical fluctuations of the charge carriers. In many analog applications the noise behavior is the main concern for the designer. In contrast to noise analyzing methods on the circuit level, physics-based methods allow to localize the major noise sources within the device and to determine their importance for the measurable terminal noise performance, supporting the determination of crucial device parameters.

In recent years increasing effort has been devoted to the numerical simulation of noise in physics-based device simulators. In most cases the noise simulation is founded on Shockley's impedance field method (IFM) [1] and its variations and generalizations. The so called *adjoint impedance field method* (AIFM) (e.g. [2]) is limited to one-carrier, passive devices due to the assumed symmetry of the transfer function of the fluctuations to the device terminals, thereby unable to distinguish majority and minority carrier noise contributions. Bonani et al. [3] reported a numerically efficient Green function approach to the Langevin equation based simulation of the impedance field method, a variation of the *direct impedance field method* (DIFM). Another generalization of the IFM is the *transfer impedance field method* (TIFM) developed by Van Vliet et al. in [4] (see also [5]). Very recently, RF noise sources were derived from bulk Monte Carlo simulations [6].

The paper is structured as follows. Section 2 gives a brief review of the direct impedance field method, the RF noise sources, and the transport equations. The dc calibration with details of the applied physical models and parameters are presented in Sect. 3. The noise simulations are described in Sect. 4, including subsections on hot electron effects, thermal hole noise in the substrate, and the comparison of basic noise quantities simulated in the drift-diffusion (DD) and energy-balance (EB) transport models. Here, we also use noise sources generated by bulk full-band Monte Carlo (FBMC) simulations of the autocorrelation function of velocity fluctuations for comparison. Finally, the results are summarized and discussed in the Conclusions.

2. Direct Impedance Field Method

The noise analysis is based on the Langevin equation using a Green function approach as described in [3]. This technique allows the modeling of small-signal perturbations of the underlying transport model and to compute the voltage fluctuations at the terminals in terms of correlation spectra due to the local microscopic noise sources in the device. In the Langevin approach the phenomenogical PDEs $F(D,u)=0$ describing the physical system are perturbed by small excitations, random forces or "Langevin forces" s, and take the form

$$L(D,u_0)\delta u = s \tag{1}$$

after linearization and under the assumption of small perturbations, where u_0 is a solution of the unperturbed system. With the Green function G of Eq. (1) which satisfies $L(D,u_0)G(r,r_1;t,t_1)=\delta(t-t_1)\delta(r-r_1)$, the solution δu can formally be written as

$$\delta u(r,t) = \int_\Omega \int_{-\infty}^{t} G(r,r_1;t,t_1)\, s(r_1,t_1)\, dt_1 dr_1 \,.$$

Manuscript received September 4, 2002.

[†]The authors are with Institut für Integrierte Systeme, ETH Zürich, Gloriastrasse 35, CH-8092 Zürich, Switzerland.

[††]The authors are with ISE Integrated Systems Engineering AG, Balgriststrasse 102, CH-8008 Zürich, Switzerland.

[†††]The author is with AMD Saxony, Wilschdorfer Landstrasse 101, D-01109 Dresden, Germany.

a) E-mail: schenk@iis.ee.ethz.ch

For time invariant Green functions, i.e. if $G(r, r_1; t, t_1) = G(r, r_1; t - t_1, 0)$, a frequency domain analysis becomes possible, and Fourier transformation implies

$$\delta u(r, \omega) = \int_\Omega G(r, r_1; \omega)\, s(r_1, \omega)\, dr_1. \tag{2}$$

This approach is applied to the perturbed EB transport model where $u = (\psi, n, p, T_n, T_p)$. We use the formulation proposed by Bløtekjær [7], which is one of the options in the general-purpose device simulator DESSIS$_{-\mathrm{ISE}}$ [8]. If the expressions for current and energy-current densities are inserted into the conservation equations of this transport model, the vector of the Langevin sources s in Eq. (1) becomes

$$s = \begin{pmatrix} 0 \\ \xi_n + \nabla \cdot \underline{\xi}_{j_n} \\ \xi_p - \nabla \cdot \underline{\xi}_{j_p} \\ \xi_{w_n} - \nabla \cdot \underline{\xi}_{S_n} + \nabla \cdot \left(\frac{5}{2} \frac{k_\mathrm{B} T_n}{q} \underline{\xi}_{j_n} \right) - q \nabla\psi \cdot \underline{\xi}_{j_n} \\ \xi_{w_p} - \nabla \cdot \underline{\xi}_{S_p} - \nabla \cdot \left(\frac{5}{2} \frac{k_\mathrm{B} T_p}{q} \underline{\xi}_{j_p} \right) - q \nabla\psi \cdot \underline{\xi}_{j_p} \end{pmatrix}. \tag{3}$$

For simplicity, we neglect generation-recombination completely, i.e. $\xi_n = \xi_p = \xi_{w_n} = \xi_{w_p} = 0$. Inserting Eq. (3) into Eq. (2), integrating by parts with the b.c. that the normal component of the fluctuating currents is zero on the domain boundary and introducing *vector* Green functions $\underline{G}^\beta_\alpha(r, r_1; \omega) = \nabla_{r_1} G^\beta_\alpha(r, r_1; \omega)$, Eq. (2) can be written as

$$\delta u_\beta(r, \omega) = \sum_{\alpha = n,p} \int_\Omega dr_1 \left\{ \underline{\Gamma}^\beta_\alpha(r, r_1; \omega) \cdot \underline{\xi}_{j_\alpha} + \right. \\ \left. + \underline{G}^\beta_{w_\alpha}(r, r_1; \omega) \cdot \underline{\xi}_{S_\alpha} \right\} \tag{4}$$

with the abbreviation

$$\underline{\Gamma}^\beta_\alpha = (-1)^{\delta_{\alpha n}} \left[\underline{G}^\beta_\alpha + \underline{G}^\beta_{w_\alpha} \frac{5}{2} \frac{k_\mathrm{B} T_\alpha}{q} \right] - \underline{G}^\beta_{w_\alpha} q \nabla\psi. \tag{5}$$

The superscript at the Green functions denotes the fluctuating variable, whereas the subscript labels the equation of the transport model. Under the assumption of spatially independent noise sources the noise *voltage* correlation spectra result in

$$S_{\psi,\psi}(r, r'; \omega) = \sum_{\alpha,\beta = n,p} \int_\Omega dr_1 \\ \cdot \left[\underline{\Gamma}^\psi_\alpha(r, r_1; \omega) \underline{\underline{K}}_{j_\alpha, j_\beta}(r_1; \omega) \underline{\Gamma}^{\psi *}_\beta(r', r_1; \omega) \right. \\ + \underline{\Gamma}^\psi_\alpha(r, r_1; \omega) \underline{\underline{K}}_{j_\alpha, S_\beta}(r_1; \omega) \underline{G}^{\psi *}_{w_\beta}(r', r_1; \omega) \\ + \underline{G}^\psi_{w_\alpha}(r, r_1; \omega) \underline{\underline{K}}_{S_\alpha, j_\beta}(r_1; \omega) \underline{\Gamma}^{\psi *}_\beta(r', r_1; \omega) \\ \left. + \underline{G}^\psi_{w_\alpha}(r, r_1; \omega) \underline{\underline{K}}_{S_\alpha, S_\beta}(r_1; \omega) \underline{G}^{\psi *}_{w_\beta}(r', r_1; \omega) \right], \tag{6}$$

where $\underline{\underline{K}}$ are the local flux noise sources, e.g.

$$\underline{\underline{K}}_{j_\alpha, S_\beta}(r_1; \omega)\, \delta(r_1 - r_1') = 2\, \overline{\underline{\xi}_{j_\alpha} \underline{\xi}^*_{S_\beta}}. \tag{7}$$

Only components of the matrix-valued Green function with superscript ψ are needed, thus we omit this superscript in the following.

From Eq. (6) we obtain the auto-correlation spectrum $S^c_V(\omega)$ for a contact c at location r using $r = r'$ and the cross-correlation spectrum $S^{cc'}_V(\omega)$ for contact c at r and a second contact c' at r'. It has been shown that the Green function approach for the Langevin equation is equivalent to Shockley's Impedance Field Method [9].

The main problem is to find proper analytical expressions for the flux noise sources (Eq. (7)). Since electron-hole scattering is negligible in MOSFETs, we have $\underline{\underline{K}}_{j_\alpha, j_\beta} = \underline{\underline{K}}_{j_\alpha, j_\alpha}\, \delta_{\alpha\beta}$ etc. It has been shown by the Chapman-Enskog method applied to the homogeneous Boltzmann equation with constant electric field [10], that

$$K_{j_n, j_n; lm}(r_1; 0) = 4q^2 n(r_1) D_n(r_1)\, \delta_{lm} \tag{8}$$

$$K_{j_p, j_p; lm}(r_1; 0) = 4q^2 p(r_1) D_p(r_1)\, \delta_{lm} \tag{9}$$

if electron-electron collisions are neglected. In the simulation with DESSIS$_{-\mathrm{ISE}}$ [8] the conductivity contains the mobility, the choice of which depends on the transport model used (DD or EB). Parameters that affect the dependence on normal and longitudinal electric field or on carrier temperature in the EB case, were carefully calibrated for a best fit between simulated and measured transfer characteristics. We use Eqs. (8) and (9) and replace e.g. for electrons $D_n(r_1) \rightarrow k_\mathrm{B} T_\mathrm{L}\, \mu_n(E_\parallel, E_\perp)/q$ in the DD case and $D_n(r_1) \rightarrow k_\mathrm{B} T_n\, \mu_n(T_n, E_\perp)/q$ in the EB case, where T_n is the local electron temperature of the EB model.

For comparison we computed the autocorrelation function of velocity fluctuations by bulk FBMC simulations for ⟨110⟩ silicon at 300 K and stored the results as function of field, density, and doping concentration. Details of the scattering model can be found in Ref. [12]. Since we assume that $\delta j_n = qn\delta v_n$, instead of Eq. (8) the electron diffusion noise source is then given by

$$K_{j_n, j_n; l} = \frac{4}{n} \int_0^\infty dt\, \left\langle \delta j^l_n(0)\, \delta j^l_n(t) \right\rangle, \tag{10}$$

where $l = (\parallel, \perp)$ denotes the component either parallel or perpendicular to the field vector and $\langle ... \rangle$ is the ensemble average. In Sect. 4 we will use the noise source Eq. (10) together with the vector Green functions from the DD simulations to arrive at noise figures which can be directly compared with those from the conventional DD noise simulation. Although Eq. (10) is superior to noise sources based on the Einstein relation, it has to be pointed out that the bulk FBMC results can be applied to a MOSFET channel at the utmost in the sub-

threshold regime, but not in the on-state, where channel effects like surface-roughness scattering determine the resistance. Furthermore, if the FBMC noise source is interpreted as function of the local electric field in the device, the assumption that the field vector is parallel to $\langle 110 \rangle$ is only fulfilled in the drain junction near the interface. Hence, using Eq. (10) will serve mainly to demonstrate, how much the simulated noise figure depends on the form of the noise source.

An expression for $K_{S_\alpha,S_\alpha}(r_1;0)$ valid for an isotropic fluid at thermodynamic equilibrium was derived by Bixon and Zwanzig [13] by using the first Chapman-Enskog approximation:

$$K_{S_\alpha,S_\alpha;lm}(r_1;0) = 2k_\mathrm{B}T_\mathrm{L}^2\,\kappa_\alpha\,\delta_{lm} \quad (\alpha = n,p). \quad (11)$$

The cross source K_{j_α,S_α} is zero for an isotropic fluid [14]. In the EB simulations we use

$$K_{S_\alpha,S_\alpha;lm}(r_1;\omega) = 2k_\mathrm{B}T_\alpha^2\,\kappa_\alpha\,\delta_{lm} \quad (\alpha = n,p) \quad (12)$$

with the thermal conductivities κ_α expressed by the Wiedemann-Franz law, i.e. containing the mobility $\mu_\alpha(T_\alpha, E_\perp)$. The cross correlation functions are neglected in accordance with the isotropic transport model used in the simulation.

3. DC Simulation

The noise analysis with DESSIS$_{-\mathrm{ISE}}$ [8] is performed both in the DD and the EB transport model. A careful dc calibration resulted in an almost perfect agreement of the corresponding $I_\mathrm{ds} - V_{gs}$-characteristics as shown in Fig. 1. Carrier-temperature driven impact ionization and high-field saturation [15] with default parameters were used in the EB scheme. Energy relaxation times were chosen as $\tau_{e,n} = 0.3\,\mathrm{ps}$ and $\tau_{e,p} = 0.2\,\mathrm{ps}$. A parameter in the channel mobility model of Lombardi [16] which describes acoustic phonon scattering was increased by one order of magnitude compared to the default value. For the drift-diffusion simulations, field-driven velocity saturation was applied using the Caughey/Thomas model [17] with default parameters.

Despite almost identical $I_\mathrm{ds} - V_{gs}$-curves which can always be achieved by changing parameters in the above-mentioned physical models, the internal field and density profiles along and perpendicular to the channel differ considerably (Fig. 2 and Fig. 3). These differences are, besides the different noise sources, the cause of differences in the simulated noise quantities.

4. Noise Simulations

In the noise simulations with DESSIS$_{-\mathrm{ISE}}$ [8] all electrodes except *drain* and *gate* were always kept short-cut to ac-ground. The *drain* and *gate* terminals were always kept ac-open-circuited to enable the extraction of the

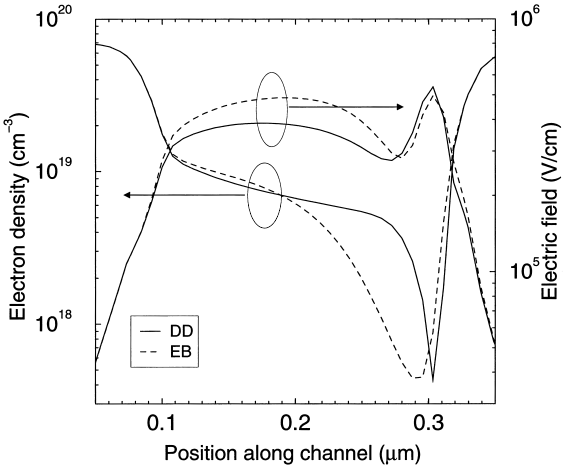

Fig. 2 Electron density (left) and absolute value of electric field (right) along the channel 1 nm below the Si-SiO$_2$ interface. Bias: $V_\mathrm{ds} = 2.5\,\mathrm{V}$, $V_{gs} = 1.5\,\mathrm{V}$.

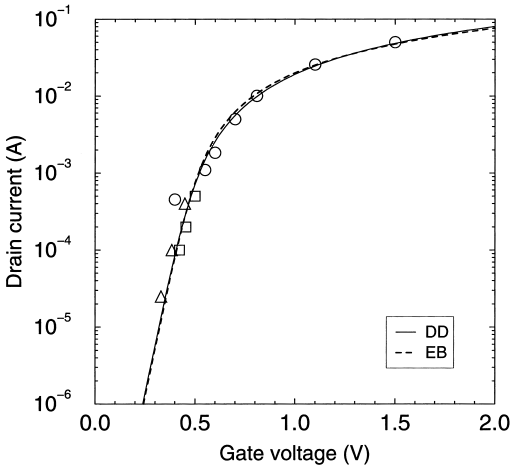

Fig. 1 Simulated $I_\mathrm{ds} - V_{gs}$-characteristics of a 0.25 μm nMOSFET in the drift-diffusion (solid) and energy-balance transport model (dashed) in comparison with experimental data (symbols). Bias: $V_\mathrm{ds} = 2.5\,\mathrm{V}$.

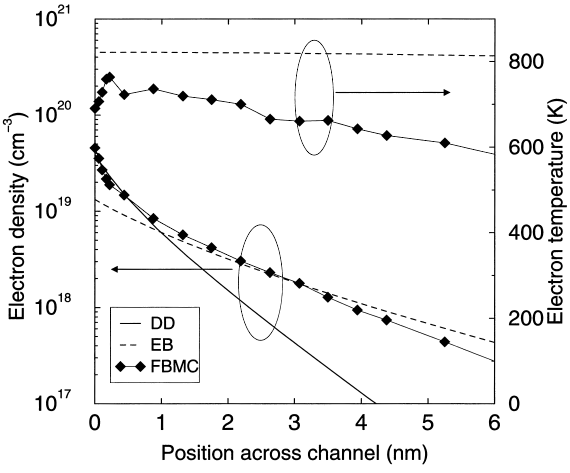

Fig. 3 Electron density (left) and electron temperature (right) perpendicular to the channel in the middle of the device. Bias: $V_\mathrm{ds} = 2.5\,\mathrm{V}$, $V_{gs} = 1.5\,\mathrm{V}$.

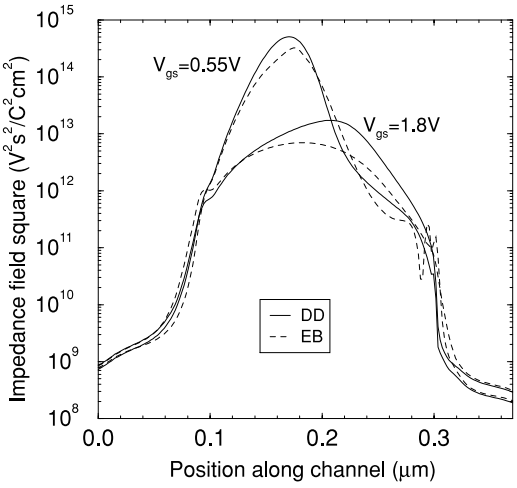

Fig. 4 Square modulus of the electron vector Green function along the channel of the 0.25 μm nMOSFET 1 nm below the Si-SiO_2 interface in the drift-diffusion (solid) and energy-balance transport model (dashed) for different V_{gs}. Bias: $V_{ds} = 2.5\,\mathrm{V}$, frequency: $f = 4\,\mathrm{GHz}$.

noise voltage spectra. Together with the Y-parameters, this is sufficient to compute all noise charateristics of the device.

In order to check the validity of the noise implementation, we computed the noise current spectral density by means of the Nyquist theorem $S_I^d = 4k_\mathrm{B}T\,\mathrm{Re}(Y_{22})$ using Y_{22} from the ac analysis and compared it with the result of the DIFM. The agreement was excellent both in the DD as well as in the EB case (relative error at $V_{ds} = 0\,\mathrm{V}$, $V_{gs} = 1.5\,\mathrm{V}$ was 0.1% for DD and 1% for EB!). Figure 4 shows a comparison of the square modulus of the vector Green functions $\underline{G}_n(r_\mathrm{drain}, r; f = 4\,\mathrm{GHz})$ in the DD case and $\underline{\Gamma}_n(r_\mathrm{drain}, r; f = 4\,\mathrm{GHz})$ in the EB case along the channel at $V_{ds} = 2.5\,\mathrm{V}$ and two values of V_{gs}: 0.55 V (subthreshold) and 1.8 V (on-state). One observes higher maximum values of the vector Green function in the DD case, more pronounced in the on-state. The position of the maxima shifts from the left part of the channel towards the center as the gate voltage is increased. The values of the maxima drop by almost two orders. Both effects are related to the change of the resistivity in the channel.

4.1 Hot Electron Effects on RF Noise

Figure 5 shows a direct comparison of the spatial distributions of electron temperature and *local* drain noise voltage spectral density in the 0.25 μm nMOSFET. The latter quantity is defined by the integrand in Eq. (6). The RF diffusion noise is concentrated in the *central* part of the channel (see Fig. 5, right part), i.e. in the region of maximum resistance, mainly due to the sharp maximum of the vector Green function there as pointed out above, but *not* in the hot carrier region of the channel (i.e. not at the drain junction). The profiles of diffusion noise source and drain noise voltage spectral density along the channel in Fig. 6 prove that hot carriers have a strong effect only in the "hot spot." Here, the maximum electron temperature is about 20 times the lattice temperature at the given bias, which increases the "hot" noise source (with electron temperature instead of lattice temperature) by a factor of 20 compared to an isothermal noise source with $T = 300\,\mathrm{K}$. A certain amount of carrier heating also occurs in the central part of the channel (compare Fig. 3), because even there the longitudinal field exceeds $10^5\,\mathrm{V/cm}$. This leads to an increase of the maximum noise voltage spectral density by a factor of 2–3. Thus, the hot carrier effect under *normal* operating conditions is rather moderate due to the effective spatial separation between peak of the vector Green function and region of maximum electron temperature. Note, that vector Green function and electron density are very small in the region of hottest electrons (the brightest region 150 nm below the surface at the drain junction in Fig. 5, left part).

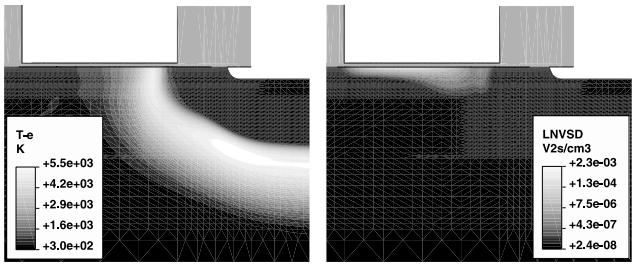

Fig. 5 Spatial distribution of the electron temperature (left) and the local RF drain noise voltage spectral density at $f = 10\,\mathrm{GHz}$ (right) in the 0.25 μm nMOSFET. Bias: $V_{ds} = 2.5\,\mathrm{V}$, $V_{gs} = 1.5\,\mathrm{V}$.

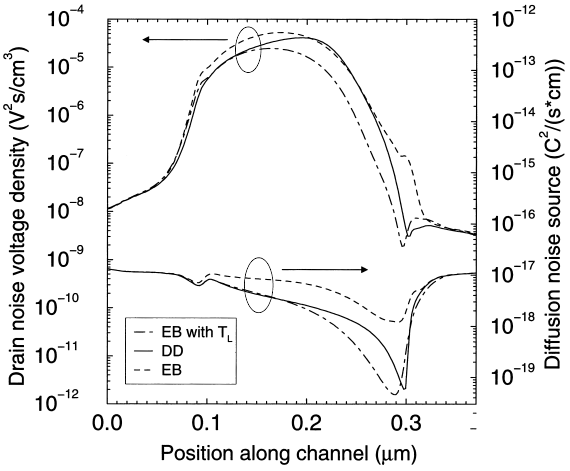

Fig. 6 Spatial distribution of the drain noise voltage spectral density (left) and the electron diffusion noise source (right) at $f = 4\,\mathrm{GHz}$ along the channel of the 0.25 μm nMOSFET 1 nm below the Si-SiO_2 interface. DD (solid), EB (dashed), and EB with $T_n \to T_\mathrm{L}$ in the noise source (dot-dashed). Bias: $V_{ds} = 2.5\,\mathrm{V}$, $V_{gs} = 1.8\,\mathrm{V}$.

We now discuss the contribution of the energy-flux fluctuations to the total diffusion noise (last term in Eq. (6) with the noise source Eq. (12)). Figure 7 compares $|\underline{G}_{w_n}|^2$ with $|\underline{G}_n|^2$ along the channel at $V_{\rm ds} = 2.5\,{\rm V}$ and $f = 4\,{\rm GHz}$. The former has sharp central minima at the peak positions of the latter, caused by a change of sign of the x-component of $\mathrm{Re}(\underline{G}_{w_n})$ and $\mathrm{Im}(\underline{G}_{w_n})$. The comparison of the noise sources in Fig. 8 shows that significant contributions from the energy-current fluctuations are restricted to the hot spot (due to the T_n^2-proportionality). But even here, the resulting drain noise voltage density is still slightly smaller than the noise density induced by current fluctuations. Since the hot spot does not dominate the terminal noise, it is already clear from the noise density profiles in Fig. 8 that the relative contribution of energy-flux fluctuations remains negligibly small. Although this conclusion is based on an expression for the noise source which is strictly valid only in equilibrium (Eq. (12)) and which uses the Wiedemann-Franz law for the thermal conductivity, it should hold generally under normal operating conditions of the MOSFET.

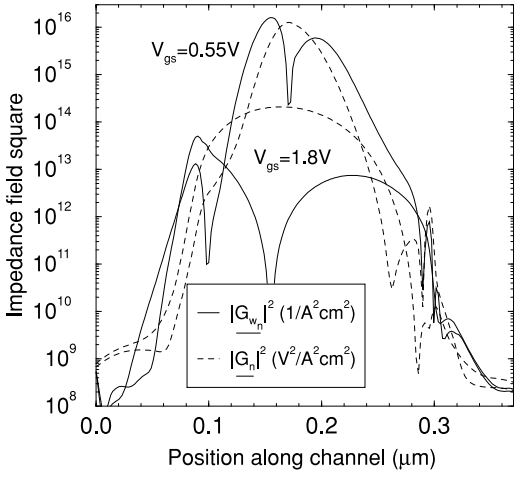

Fig. 7 Comparison of the square modulus of the electron vector Green functions $\underline{G}_{w_\eta}(r_{drain}, r; f = 4\,{\rm GHz})$ (solid) and $\underline{G}_n(r_{drain}, r; f = 4\,{\rm GHz})$ (dashed) along the channel of the $0.25\,\mu$m nMOSFET 1 nm below the Si-SiO_2 interface for different $V_{\rm gs}$. Bias: $V_{\rm ds} = 2.5\,{\rm V}$, frequency: $f = 4\,{\rm GHz}$.

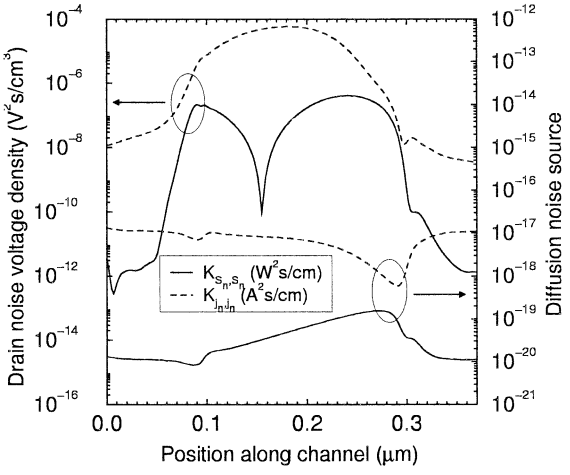

Fig. 8 Profiles of the drain noise voltage spectral densities (left) and electron diffusion noise sources (right) for energy-current fluctuations (solid) and current fluctuations (dashed) at $f = 4\,{\rm GHz}$ along the channel of the $0.25\,\mu$m nMOSFET 1 nm below the Si-SiO_2 interface. Bias: $V_{\rm ds} = 2.5\,{\rm V}$, $V_{\rm gs} = 1.8\,{\rm V}$.

4.2 Substrate Effect on Drain Noise Voltage Spectrum

If the substrate thickness of $0.5\,\mu$m used in our simulations is increased to $18\,\mu$m, thermal hole noise dominates S_V (and S_I) at frequencies below $5 \times 10^8\,{\rm Hz}$. Although in the substrate both the vector Green function and the noise source are smaller by roughly two orders of magnitude when compared to the corresponding peak values in the channel, due to the large volume of the $18\,\mu$m thick bulk region the effect accumulates and yields a dominant contribution to the total drain noise voltage spectral density (Fig. 9). The shoulder at $10^8\,{\rm Hz}$ is related to a corresponding shoulder of $\mathrm{Re}(Y^{22})$. Probably the resulting substrate resistance determines a RC time constant responsible for the effect.

In RF noise measurements it is common practice to subtract the substrate as a "pad effect" when measuring NF50 or NFmin, which could explain why the shoulder at about $10^8\,{\rm Hz}$ has never been measured (though visible in the simulation results of Ref. [19], too). However, under normal operating conditions thermal hole noise is present and cannot be ignored.

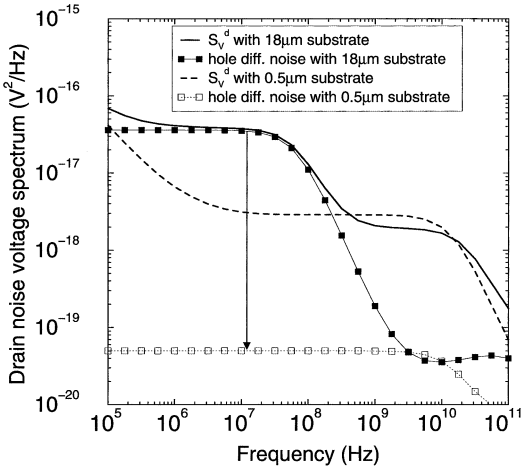

Fig. 9 Drain noise voltage spectral density of the $0.25\,\mu$m nMOSFET in the DD model at $V_{\rm ds} = 2.5\,{\rm V}$ and $V_{gs} = 1.5\,{\rm V}$ with substrate of $18\,\mu$m (solid) and $0.5\,\mu$m thickness (dashed). The arrow indicates the corresponding drop of the hole diffusion noise contribution. The low-frequency increase of S_V^d is due to flicker noise included in the simulation.

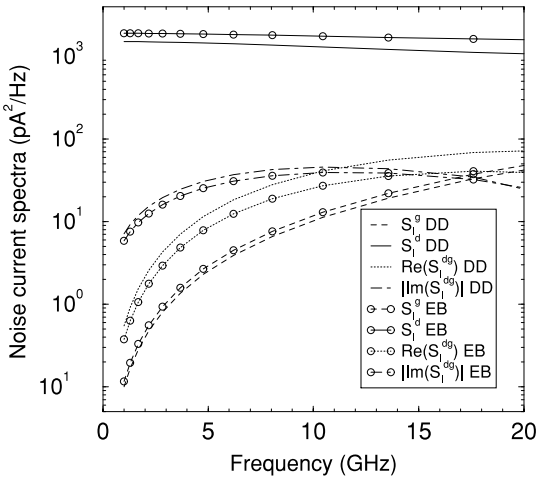

Fig. 10 Simulated noise current spectral densities S_I^{g}, S_I^{d}, $\mathrm{Re}(S_I^{\mathrm{dg}})$, and $|\mathrm{Im}(S_I^{\mathrm{dg}})|$ of the 0.25 μm nMOSFET in the drift-diffusion (no symbols) and energy-balance transport model (circles). Bias: $V_{\mathrm{ds}} = 2.5\,\mathrm{V}$, $V_{gs} = 1.8\,\mathrm{V}$.

4.3 Current Noise Spectra, NF50 and NFmin of 0.25 μm nMOSFET

The noise current spectra are given by $S_I = \hat{Y}\, S_V\, \hat{Y}^H$, where $\hat{Y}$ is the admittance matrix of the two-port. The noisy input admittance Y_S at the input (gate) has a current noise spectrum $S_I^S = 4k_{\mathrm{B}}T\mathrm{Re}(Y_{\mathrm{S}})$ and is, therefore, complemented by the input current noise source i_{S}. Simulation results of the current noise spectral densities are compared in Fig. 10 for the two transport models. The dominant drain current noise is slightly larger in the EB model. The same holds for the gate current noise, whereas the cross spectra are slightly larger in the DD model. However, the striking feature is the overall close agreement between DD and EB results. As shown above, hot electron effects are unimportant, but the maximum of the EB noise source is 2–3 times larger than for DD. Obviously, this is compensated by the smaller vector Green function (compare Figs. 4 and 6).

The noise figure NF can be derived as

$$NF = 1 + \frac{1}{S_I^{\mathrm{S}}}\left(S_I^{11} + |\alpha|^2 S_I^{22} - 2\mathrm{Re}\left(\alpha S_I^{21}\right)\right) \quad (13)$$

with $\alpha = (Y_{\mathrm{S}} + Y_{11})/Y_{21}$. It has exactly one minimum for positive real part $\mathrm{Re}(Y_{\mathrm{S}})$ of the input admittance. The simulated NF50 according to Eq. (13) for the DD and EB transport models are shown in Fig. 11. As for the noise current spectra, both transport models give similar results. They feature a decreasing behavior with respect to the gate voltage. The DD simulation in addition shows a saturation effect for large $V_{\mathrm{g}s}$. The limit of thermal noise according to the Nyquist law is shown as bold dashed curve (computed with the corresponding Y-parameters from the ac simulation). Figure 12 demonstrates the contribution of energy-current fluctuations to the total noise figure NF50. As already stated in Sect. 4, these contributions are negligible for all $V_{\mathrm{g}s}$ and reasonable drain voltages.

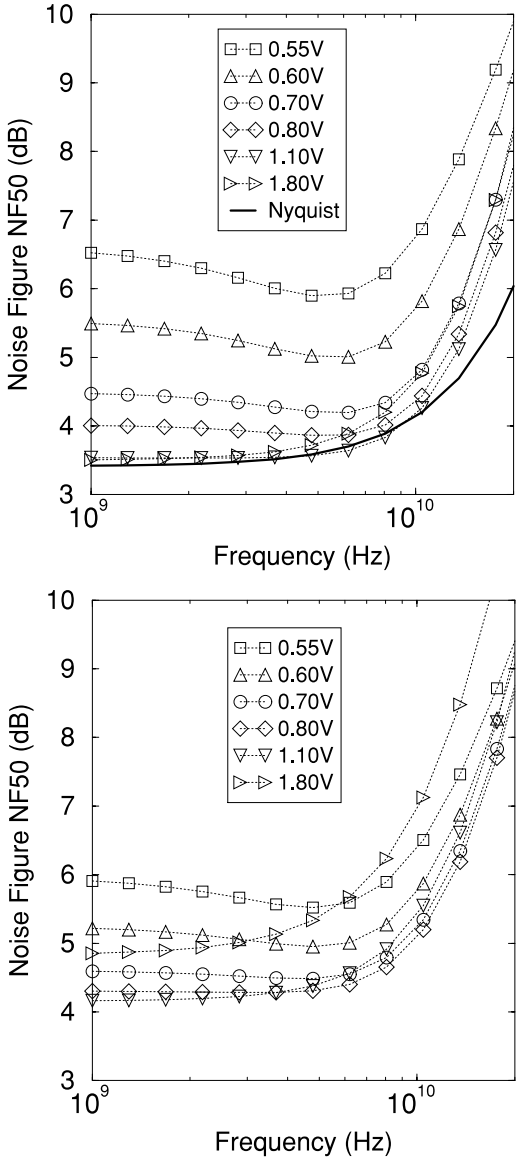

Fig. 11 Simulated NF50 of the 0.25 μm nMOSFET at $V_{\mathrm{ds}} = 2.5\,\mathrm{V}$. Gate voltages are given in the legend. Top: drift-diffusion model, bottom: energy-balance model.

In Fig. 13 we replaced the noise source based on the Einstein relation by the bulk FBMC generated noise source Eq. (10). The Green functions and all ac quantities were adopted from the DD simulation. If the local electric field in the device is used for the parametrization of the noise source (open symbols), NF50 increases drastically for all $V_{\mathrm{g}s}$. As already discussed in Sect. 2, a bulk noise source cannot be expected to describe a MOSFET in the on-state, since the resistance is dominated by channel effects. If the noise source is taken

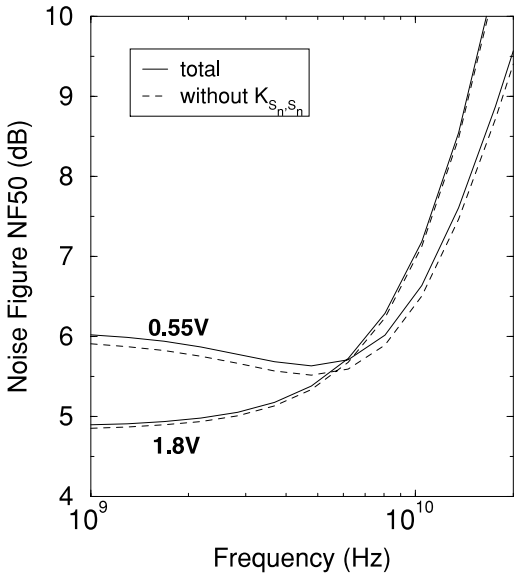

Fig. 12 Simulated total NF50 (solid curves) and NF50 without energy-current noise source (dashed curves) of the 0.25 μm nMOSFET at $V_{\rm ds} = 2.5$ V for two gate voltages.

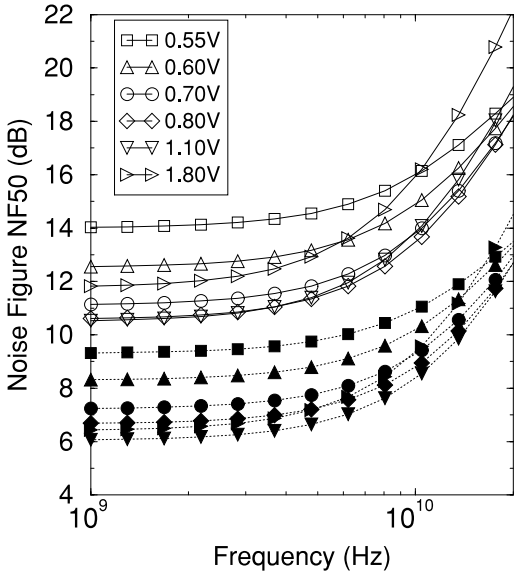

Fig. 13 Simulated NF50 of the 0.25 μm nMOSFET at $V_{\rm ds} = 2.5$ V. Gate voltages are given in the legend. Open symbols: DD with noise source from bulk FBMC as function of electric field, filled symbols: DD with noise source from bulk FBMC as function of gradient Quasi Fermi.

as function of the local gradient Quasi Fermi in the device (filled symbols), an upward shift of all curves by 2.5 dB compared to Fig. 11 is observed. These results clearly demonstrate that the correct form of the non-equilibrium noise source is crucial for the simulation of the noise figure.

5. Conclusions

Simulation of noise on the device level remains challenging from a physical point of view (non-equilibrium noise sources) but also from a numerical point of view (discretization of the vector Green functions, mesh refinement, robustness). We compared RF noise simulations of a quarter-micron nMOSFET based on the DD and the EB transport model, respectively. It could be shown that a shoulder in the noise spectrum at about 10^8 Hz is due to thermal noise of holes in the substrate. This shoulder disappears for sufficiently small substrate resistance (very thin substrate in the simulation). We also demonstrated that the carrier heating in the hot spot near the drain has only little effect on the RF noise, because this region is spatially separated from the mainly contributing central part of the channel. Hence, the "hot-carrier effect" just amounts in the warm-up of electrons in the latter part and in the corresponding increase of the local noise source there. We showed that the contribution of energy-current fluctuations to the noise figure is negligibly small under normal operating conditions. The use of non-equilibrium noise sources generated by bulk FBMC, instead of expressions based on the Einstein relation, improves the situation only in the sub-threshold regime, where the MOSFET shows sufficient bulk-like behavior. In the on-state, surface scattering determines the resistance and hence the noise figure. Here, diffusion noise is closer to thermal noise (Nyquist theorem) than in the subthreshold regime, and the Einstein relation might be a more useful concept.

For a better modeling of diffusion noise sources in MOSFETs the generation of lookup tables with FBMC including surface scattering seems to be inevitable. On the other hand, for a comparison with measured (deembedded) noise data it is not sufficient to consider the intrinsic MOSFET alone, since parasitics not covered by the simulation domain of the intrinsic device are not negligible. Quantities like NF50 and NFmin are sensitive to the Y-parameters. Therefore, a more accurate modeling of the actual measurement equivalent circuit might be necessary for a reasonable comparison between simulation and experiment.

Acknowledgement

The authors are grateful to Tatsuya Ohguro, Hideki Kimijima, and Eiji Morifuji (Toshiba Corp.) for providing experimental data on the devices studied in this paper, to Hideki Takada (Kanematsu Electronics) for his support in joint simulation projects, and to Prof. Hiroshi Iwai (Tokyo Institute of Technology) for many valuable discussions.

References

[1] W. Shockley, J.A. Copeland, and R.P. James, "The impedance field method of noise calculation in active semiconductor devices," in Quantum Theory of Atoms, Molecules and the Solid State, ed. P.-O. Loewdin, pp.537–563, Academic Press, 1966.
[2] J.-P. Nougier, "Noise in devices: Definition, modelling," in III-V Microelectronics, ed. J.-P. Nougier, vol.2 of European Materials Research Society Monographs, pp.183–238, North-Holland, 1991.
[3] F. Bonani, G. Ghione, M.R. Pinto, and R.K. Smith, "An efficient approach to noise analysis through multidimensional physics-based models," IEEE Trans. Electron Devices, vol.45, no.1, pp.261–269, Jan. 1998.
[4] K.M. van Vliet, A. Friedmann, R.J.J. Zijlstra, A. Gisolf, and A. van der Ziel, "Noise in single injection diodes. I. a survey of methods," J. Appl. Phys., vol.46, no.4, pp.1804–1823, April 1975.
[5] J.-P. Nougier, J.C. Vaissiere, D. Gasquet, and A. Motadid, "Noise sources of hot carriers in space-charge regimes," J. Appl. Phys., vol.52, no.9, pp.5683–5688, Sept. 1981.
[6] C. Jungemann, B. Neinhüs, S. Decker, and B. Meinerzhagen, "Hierarchical 2D RF noise simulation of Si and SiGe devices by Langevin-type DD and HD models based on MC generated noise parameters," IEDM 2001, IEDM, 2001.
[7] K. Bløtekjær, "Transport equations for electrons in two-valley semiconductors," IEEE Trans. Electron Devices, vol.ED-17, no.1, pp.38–47, 1970.
[8] ISE Integrated Systems Engineering AG, Balgriststrasse 102, CH-8008 Zürich, DESSIS 7.5 reference manual, 2001.
[9] T.C. McGill, M.-A. Nicolet, and K.K. Thornber, "Equivalence of the Langevin method and the impedance-field method of calculating noise in devices," Solid-State Eletron., vol.17, pp.107–108, 1974.
[10] V.L.G.S.V. Gantsevich and R. Katilius, "Theory of fluctuations in nonequilibrium electron gas," Rivista Del Nuovo Cimento, vol.2, no.5, pp.1–87, 1979.
[11] P. Golinelli, L. Varani, and L. Reggiani, "Generalization of thermal conductivity and Lorenz number to hot carrier conduction in nondegenerate semiconductors," Phys. Rev. Lett., vol.77, pp.1115–1118, 1996.
[12] F.M. Bufler, A. Schenk, and W. Fichtner, "Efficient Monte Carlo device modeling," IEEE Trans. Electron Devices, vol.47, no.10, pp.1891–1897, 2000.
[13] M. Bixon and R. Zwanzig, "Boltzmann-Langevin equation and hydrodynamic fluctuations," Phys. Rev., vol.187, no.1, pp.267–272, 1969.
[14] D. Zubarev, V. Morozov, and G. Röpke, Statistical Mechanics of Nonequilibrium Processes, Akademie-Verlag, Berlin, 1996.
[15] B. Meinerzhagen and W.L. Engl, "The influence of the thermal equilibrium approximation on the accuracy of classical two-dimensional numerical modeling of silicon submicrometer MOS transistors," IEEE Trans. Electron Devices, vol.35, no.5, pp.689–697, 1988.
[16] C. Lombardi, S. Manzini, A. Saporito, and M. Vanzi, "A physically based mobility model for numerical simulation of nonplanar devices," IEEE Trans. Comput.-Aided Des. Integr. Circuits Syst., vol.7, no.11, pp.1164–1171, 1988.
[17] D.M. Caughey and R.E. Thomas, "Carrier mobilities in silicon empirically related to doping and field," Proc. IEEE, pp.2192–2193, Dec. 1967.
[18] T. Lackner, "Avalanche multiplication in semiconductors: A modification of Chynoweth's law," Solid-State Eletron., vol.34, pp.33–42, 1991.
[19] S. Donati, M.A. Alam, K.S. Kirsch, S. Martin, M.R. Pinto, H.H. Vuong, F. Bonani, and G. Ghione, "Physics-based RF noise modeling of submicron MOSFETs," IEDM Tech. Digest, pp.81–84, 1998.

Andreas Schenk was born in 1957. He received the Dipl. Phys. degree and the Ph.D. from Humboldt University in Berlin (HUB) in 1981 and 1987, respectively. From 1987 till 1991 he was working on various aspects of the physics and simulation of optoelectronic devices. In 1991 he joined the Integrated Systems Laboratory of ETH working as a senior research/teaching assistant, where he qualified to give lectures at university in 1997 for "Physics and Modeling of Microelectronic Devices." His main activities are in the physics-based modeling for advanced simulation of submicron silicon devices and their application in the TCAD software released by ISE AG Zurich. His interests include generation-recombination, mobility, contacts, heterojunctions, many-body effects, hot carrier degradation, noise, single electron transistor modeling at device level, and quantum effects in silicon ultra-small devices. He authored and co-authored 2 books and 80 papers. Andreas Schenk is a member of the German Physical Society (DPG).

Bernhard Schmithüsen was born in Aachen, Germany, in 1962. He received his Dipl. Math. from the University of Technology Aachen (RWTH) in 1988. He worked several years on CAD software and from 1994 he concentrated on TCAD simulation at ISE AG Zurich. In 1996 he joined the Integrated Systems Laboratory at the ETH Zurich, Switzerland, working towards his Ph.D. His main interests are the discretizations and numerics of the device equations, especially in connection with gridding and grid adaptation aspects.

Andreas Wettstein received the diploma in physics from the Universität Karlsruhe in 1995 and the Ph.D. degree in engineering from the Eidgenössische Technische Hochschule in Zürich in 2000. Since then he is with ISE AG, Zürich, working as a software developer for device simulation.

Axel Erlebach was born in Dresden, Germany, in 1962. He received the Dipl. Phys. from the University of Technology Dresden, Germany, in 1987, and the Dr. rer. nat degree from the University Duisburg, Germany, in 1998. In 1987, he joined the Zentrum Mikroelektronik Dresden where he has worked on the simulation and development of DRAMs. From 1991 to 1997 he worked with the FhG Institute of Microelectronic Circuits and Systems Dresden on simulation of semiconductor devices and processes, micromechanical systems, sensors, and actuators. He is currently with ISE AG Zurich where he is working on calibration and simulation of microelectronic processes and devices.

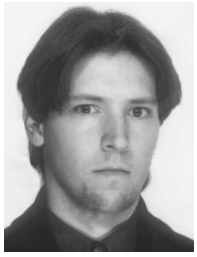

Simon Brugger received his Diploma in physics from the ETH Zürich in 2000. Since graduation he has been working at the Integrated Systems Laboratory of the ETH in the area of silicon devices. His professional interests include semiconductor device physics, applied mathematics, and Monte Carlo simulation.

Fabian Bufler studied physics at the TU Braunschweig and RWTH Aachen (both Germany) including an academic year at the Université de Grenoble I (France) with a scholarship of the Studienstiftung des deutschen Volkes and received the Dipl.-Phys. degree in 1992. Afterwards he joined the Institut für Theoretische Elektrotechnik, RWTH Aachen, and moved in 1995 together with the group of Prof. B. Meinerzhagen to the Institut für Theoretische Elektrotechnik und Mikroelektronik, Universität Bremen (Germany), where he received his doctor's degree in 1997. Since then he is with the Institut für Integrierte Systeme, ETH Zürich, working in the field of TCAD on Monte Carlo device modeling and transport theory.

Thomas Feudel was born in Olbernhau, Germany, in 1956. He received the Dipl.-Ing. and Dr.-Ing. degrees in electrical engineering from the Technical University of Chemnitz, Germany, in 1983 and 1991, respectively. In 1983 he joined the Zentrum Mikroelektronik Dresden, Germany, where he was engaged in process simulation and development of semiconductor technologies. From 1992 to 1996 he worked for the Swiss Federal Institute of Technology, Zurich, Switzerland, and till 1999 for ISE Integrated Systems Engineering AG. He is now with AMD's Fab30 in Dresden. His current interests are in process and device simulation, characterization and process integration.

Wolfgang Fichtner received the Dipl.Ing. degree in physics and the Ph.D. degree in electrical engineering from the Technical University of Vienna, Austria, in 1974 and 1978, respectively. From 1975 to 1978, he was an Assistant Professor in the Department of Electrical Engineering, Technical University of Vienna. From 1979 through 1985, he worked at AT&T Bell Laboratories, Murray Hill, NJ. Since 1985 he is Professor and Head of the Integrated Systems Laboratory at the Swiss Federal Institute of Technology (ETH). In 1993, he founded ISE Integrated Systems Engineering AG, a company in the field of technology CAD. Wolfgang Fichtner is a Fellow of the IEEE and a member of the Swiss National Academy of Engineering.